Structural Engineering and Mechanics, *Vol. 62, No. 5 (2017) 619-629*
DOI: https://doi.org/10.12989/sem.2017.62.5.619

Large deformation modeling of flexible manipulators to determine allowable load

Habib Esfandiar*[1], Moharam H. Korayem[2a] and Mohammad Haghpanahi[2a]

[1]*Department of Mechanical Engineering, Firoozkooh Branch, Islamic Azad University, Firoozkooh, Iran*
[2]*Department of Mechanical Engineering, Iran University of Science and Technology, Tehran, Iran*

(Received April 6, 2016, Revised November 29, 2016, Accepted January 5, 2017)

Abstract. This paper focuses on the study of complete dynamic modeling and maximum dynamic load carrying capacity computation of N-flexible links and N-flexible joints mobile manipulator undergoing large deformation. Nonlinear dynamic analysis relies on the Timoshenko theory of beams. In order to model the system completely and precisely, structural and joint flexibility, nonlinear strain-displacement relationship, payload, and non-holonomic constraints will be considered to. A finite element solution method based on mixed method is applied to model the shear deformation. This procedure is considerably more involved than displacement based element and shear deformation can be readily included without inducing the shear locking in the element. Another goal of this paper is to present a computational procedure for determination of the maximum dynamic load of geometrically nonlinear manipulators with structural and joint flexibility. An effective measure named as Moment-Height Stability (MHS) measure is applied to consider the dynamic stability of a wheeled mobile manipulator. Simulations are performed for mobile base manipulator with two flexible links and joints. The results represent that dynamic stability constraint is sensitive when calculating the maximum carrying load. Furthermore, by changing the trajectory of end effector, allowable load also changes. The effect of torsional spring parameter on the joint deformation is investigated in a parametric sensitivity study. The findings show that, by the increase of torsional stiffness, the behavior of system approaches to a system with rigid joints and allowable load of robot is also enhanced. A comparison is also made between the results obtained from small and large deformation models. Fluctuation range in obtained figures for angular displacement of links and end effector path is bigger for large deformation model. Experimental results are also provided to validate the theoretical model and these have good agreement with the simulated results.

Keywords: structural and joint flexibility; large deformation; dynamic stability; joint deformation; mixed finite element

1. Introduction

The introduction divides to three parts including definition and importance of subject, explanation of references, and the main contribution of this study.

In many industrial applications such as high speed assembly and heavy load carrying, the joint flexibility exists in most manipulators due to harmonic drives, torque transducers, or drive belts that usually neglected to analysis of such flexible joint systems (Desai and Kumar 1999). To determine Dynamic Load Carrying Capacity (DLCC) for flexible manipulator, accurate modeling of manipulator and load dynamics is a prerequisite. Therefore, it is necessary to extract the dynamic equations of manipulators considering the nonlinear strain-displacement relationship and both structural and joint flexibility. Many researchers have investigated the dynamic behavior of robotic manipulators considering rigid links and elastic joints, flexible links and rigid joints or flexible links and flexible joints. Most of the investigations in dynamic analysis of manipulators with both structural and joint flexibility have been confined to manipulators undergoing small deformation.

A survey of the literature related to dynamic analyses of flexible robotic manipulators has been carried out by Dwivedy and Eberhard (2006). Both link and joint flexibility are considered and an effort has been made to critically examine the methods used in these analyses, their advantages and shortcomings and possible extension of these methods to be applied to a general class of problems. Sweet and Good (1984) determined experimentally that joint flexibility exists in most manipulators in drive transmission systems. Subudhi and Morris (2002) presented a dynamic modeling technique for a manipulator with multiple flexible links and flexible joints, based on a combined Euler-Lagrange formulation and assumed modes method. In a similar work, Lin and Gogate (1989) derived the dynamics of a manipulator with flexible links and flexible joints using Hamilton's principle. Yang and Donath (1988) shown that both link and joint flexibility need to be incorporated in the modeling to achieve good trajectory tracking and quick damping of end tip vibrations, because flexible deformations produced by joints and links make it difficult for the end effector to track a prescribed trajectory accurately. Yue *et al*. (1997) proposed a finite element model for the link and torsional spring model for the joint to

*Corresponding author, Ph.D.
E-mail: habibesfandiar2014@gmail.com
[a]Ph.D.

ISSN: 1225-4568 (Print), 1598-6217 (Online)

analyze a planar 3R manipulator. Ailon (1998) considered the flexibility of the electric drive for the analysis of flexible manipulator. Yuan and Lin (1990) considered N-flexible links and joints and modeled the joints by torsional springs.

Dynamic modeling of flexible manipulators with large deformation based on displacement formulation has become a very important research subject in many fields. Nonlinear modeling for flexible multi-body system with large deformation using the absolute nodal coordinates investigated to describe the displacement, and variational motion equations of a flexible body derived on the basis of the geometric nonlinear theory (Dombrowski 2002, Kubler *et al*. 2003, Iwai 2003, Vallejo *et al*. 2003, Shabana 1998, Dmitrochenko 2008). Liu *et al*. (2007) proposed a hybrid-coordinate formulation, which is suitable for flexible multi-body systems with large deformation. Based on exact strain-displacement relation, equations of motion for flexible multi-body system are derived by using virtual work principle. Bayo (1989) used finite element method to deal with multi-link flexible manipulators considering Timoshenko beam theory and including nonlinear Coriolis and centrifugal effects for the elastic behavior. An iterative solution scheme is proposed for finding the desired joint torques where the solution of each linearization is carried out in frequency domain. Aarts and Jonkera (2002) proposed the modal integration method for analyzing the dynamic behavior of multi-link planar flexible manipulators. A nonlinear finite element method is employed to derive the equations of motion in terms of a mixed set of generalized coordinates of the manipulator. Using a perturbation method, the vibrational motion of the manipulator is modeled as a first order perturbation of the nonlinear nominal rigid link motion. Analysis of the motion indicated that the perturbation method is accurate and efficient, even for quite large deformations. Korayem and Basu (1994) introduced a new method of determining DLCC for flexible joint manipulators subject to both actuator and end effector deflection constraints. Thomas *et al*. (1985) used the load capacity as a criterion for sizing the actuators at the design stage for robot manipulators. In this study, piecewise rigid links and joints were assumed. Wang and Ravani (1988) indicated that the maximum allowable load of a fixed base manipulator on a given trajectory is primarily constrained by the joint actuator torque and its velocity characteristic. Korayem *et al*. (2005) described a computational technique for obtaining the maximum load carrying capacity of robotic manipulators with joint elasticity while considering different base positions. In another work, Korayem *et al*. (2010) determined the maximum allowable dynamic load for geometrically nonlinear manipulators with a predefined trajectory, using the finite element method. In their study, a flexible link and rigid joint planar manipulator has been investigated. Yue and Tso (2001) computed the maximum payload of redundant manipulators using a finite element method for describing the dynamics of a system. Korayem and Shokri (2008) developed an algorithm for determining the allowable dynamic load of the 6-UPS Stewart platform manipulator. Korayem and Heidari (2007) presented a general strategy for finding the maximum DLCC of flexible link mobile manipulators. The main constraints used for the proposed algorithm are the actuator torque capacity and the accuracy of end effector during motion on a given trajectory. In another work, the problem of establishing the load carrying capacity of mobile base manipulators operated by limited force or torque actuators has been presented by Korayem and Ghariblu (2007). It has been shown the maximum allowable load on a given load trajectory is a function of base position. Some researchers have studied the stability of mobile manipulators. Some earlier works discussed only static stability (Fukuda 1992, Papadopoulos and Ray 1996, Ghasempoor and Sepehri 1995), but others were concerned with dynamic stability (Huang *et al*. 2000, Kim 2002).

The main contribution of this work is the development of complete and efficient model and DLCC determination for N-flexible links and N-flexible joints mobile manipulator undergoing large deformation. The mixed finite element method which is able to consider the full nonlinear dynamic of a manipulator with both structural and joint flexibility and it can adequately model the shear deformation without being locked, is applied to derive the dynamic equations (Beirao *et al*. 2012). Then, a method for determination of the maximum allowable dynamic load for a specific trajectory is explained. The paper is thus organized in the following sections: In section 2, the mechanical and kinematical descriptions of the mobile manipulator system are described. The kinetic and potential energy of the system are obtained too. Section 3 tries to drive the dynamic equations of motion considering the mixed finite element formulation. An algorithm is proposed for determining the maximum DLCC on a given trajectory in section 4. The computational simulations are performed in section 5. The comparison between the numerical and experimental results is illustrated to verify the method proposed in section 6 and in the last section the final conclusions are considered.

2. Kinematical descriptions

In this section, the kinematics of the N-flexible links and N-flexible joints manipulator undergoing large deformation mounted on a mobile platform will be considered (Fig. 1). A payload is to be carried at the tip of the links and this subject is motivated by modeling of N-flexible links and N-flexible joints manipulators together with tip mass. In this study, the effects of shear deformation and rotary inertia are considered and the Timoshenko beam theory (TBT) is applied. Frame $\{X_0 Y_0 Z_0\}$ is the inertial reference frame, $\{X_i Y_i Z_i\}$ is a coordinate system attached to ith link. It is assumed that the elasticity at the ith joint can be modeled as a linear torsional spring with constant K_i. Vectors $\theta = \{\theta_1, \theta_2, \ldots, \theta_N\}$ as the link angle and $\theta_m = \{\theta_{m1}, \theta_{m2}, \ldots, \theta_{mN}\}$ as the rotor angle are defined for the multi-flexible link and flexible joint manipulator. The lateral deflection and shear angle are presented by $w(x)$ and $\beta(x)$, respectively. The wheeled mobile base moves on the

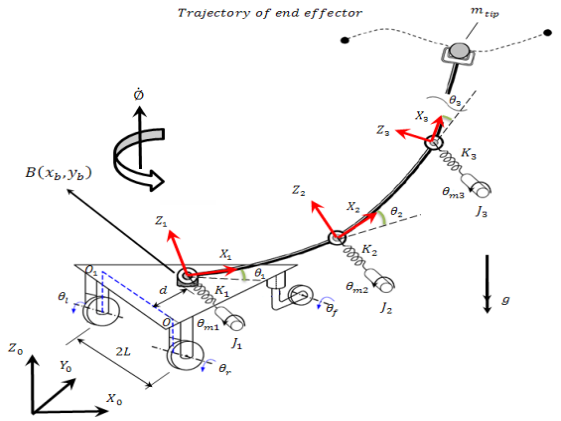

Fig. 1 N-flexible links and N-flexible joints manipulator with mobile base

ground, subject to non-holonomic constraints. The mobile platform can either move in the direction of (x_b, y_b) or rotate about the Z_b. Symbols mentioned in Figs. 1-2 have been clarified in Nomenclature.

2.1 Non-holonomic constraints for a mobile manipulator

The first constraint restricts the velocity of the mobile platform to be zero in the direction $(\overrightarrow{oo_1})$ through two axial center lines of driving wheels

$$-\dot{x}_b \sin\phi + \dot{y}_b \cos\phi - d\dot{\phi} = 0 \tag{1}$$

The other two constraints are included with assumption of no-slipping of each rolling wheel in the forward directions, and the velocity of the driving wheels can be expressed as

$$\begin{aligned} \dot{x}_b \cos\phi + \dot{y}_b \sin\phi - L\dot{\phi} &= r\dot{\theta}_l \\ \dot{x}_b \cos\phi + \dot{y}_b \sin\phi + L\dot{\phi} &= r\dot{\theta}_r \end{aligned} \tag{2}$$

2.2 Description of displacement and kinetic energy

The position vector of an infinitesimal element on the ith link located at a distance $0 \le x_i \le l_i$ relatively to the $\{X_0 Y_0 Z_0\}$ reference frame for mobile base model can be expressed by (Fig. 2)

$$\begin{aligned} &\vec{d}_i(x_i,t) = x_b\vec{I} + y_b\vec{J} + \sum_{j=0}^{i-1}\vec{P}_j(l_j,t) + \vec{P}_i(x_i,t) \\ &\vec{P}_i(x_i,t) = \begin{pmatrix} x_i\cos(\theta_{i-1}+\theta_i)\cos\phi - \\ w_i(x_i,t)\sin(\theta_{i-1}+\theta_i)\cos\phi \end{pmatrix}\vec{I} + \\ &\begin{pmatrix} x_i\cos(\theta_{i-1}+\theta_i)\sin\phi - \\ w_i(x_i,t)\sin(\theta_{i-1}+\theta_i)\sin\phi \end{pmatrix}\vec{J} + \\ &(x_i\sin(\theta_{i-1}+\theta_i) + w_i(x_i,t)\cos(\theta_{i-1}+\theta_i))\vec{K} \\ &i = 1,2,\ldots,N \quad , \quad \vec{P}_0 = 0 \quad and \quad \theta_0 = 0 \end{aligned} \tag{3}$$

where I, J, K are the unit vectors along the X_0, Y_0 and Z_0 axis, respectively. The kinetic energy of the flexible mobile manipulator involves kinetic energy of N-flexible links (T_m), kinetic energy of tip mass (T_{tip}), kinetic energy of motors (T_{motor}), and mobile base's kinetic energy (T_{base}) as

$$\begin{aligned} T_m &= \sum_{i=1}^{N} T_{i,m} \quad , \quad T_{i,m} = \frac{1}{2}\int \rho_i \left(\dot{d}_i^T(x_i,t)\cdot\dot{d}_i(x_i,t)\right)dv_i \\ T_{tip} &= \frac{1}{2} m_{tip}\left(\dot{d}_{tip}^T\cdot\dot{d}_{tip}\right) \\ T_{motor} &= \frac{1}{2}\sum_{i=1}^{N} J_i\dot{\theta}_{mi}^2 \\ T_{base} &= \frac{1}{2} m_{base}\left(\dot{x}_b^2+\dot{y}_b^2\right) + \frac{1}{2} I_{base}\dot{\phi}^2 + \frac{1}{2} J_r\dot{\theta}_r^2 + \frac{1}{2} J_l\dot{\theta}_l^2 \end{aligned} \tag{4}$$

The position vector of end effector relatively to the $\{X_0 Y_0 Z_0\}$ reference frame can be derived by

$$\vec{d}_{tip} = x_b\vec{I} + y_b\vec{J} + \sum_{j=1}^{N}\vec{P}_j(l_j,t) \tag{5}$$

2.3 Nonlinear strain-displacement relationship and potential energy

If the displacements are large enough, we must use the Green-Lagrange strain and the 2nd Piola-Kirchoff stress tensors to account for large deformation. For Timoshenko theory of beams, unknown variables are the transverse deflection $w(x)$, and the rotation $\beta(x)$. The components of displacement field across the beam height are

$$\begin{aligned} u_X &= -Z\sin\beta(x) \\ u_Y &= 0 \\ u_Z &= w(x) + Z\cos\beta(x) \end{aligned} \tag{6}$$

Nonzero Green-Lagrange strain tensor is

$$\begin{aligned} &E_{XX} = E^0 + ZK^b \Rightarrow \begin{cases} E^0 = \frac{1}{2}\left(\frac{\partial w}{\partial x}\right)^2 \\ K^b = -\left(\frac{\partial\beta}{\partial x}\right)\left[\cos\beta + \left(\frac{\partial w}{\partial x}\right)\sin\beta\right] \end{cases} \\ &E_{XZ} = \frac{1}{2}\left[-\sin\beta + \left(\frac{\partial w}{\partial x}\right)\cos\beta\right] = \Gamma \end{aligned} \tag{7}$$

where E^0 and Γ are strains which are constant on the cross-section and K^b measures change in rotation (curvature)

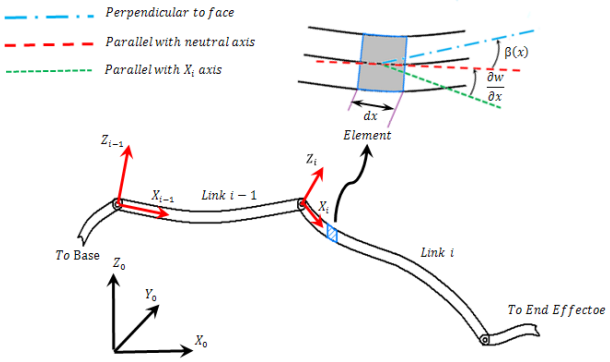

Fig. 2 Manipulator with flexible links

of the cross-sections. Assuming a linear constitutive relation, the strain energy can be obtained as

$$SE = \frac{1}{2}\int_{v} [E_{ij}]^T [S_{ij}] dV \tag{8}$$

Expanding above integral, and since z is measured from the neutral axis, all integrals of the form $\int ZdA$ must vanish. To express the strain potential energy of the whole system, we get

$$SE = \frac{1}{2}\sum_{i=1}^{N}\int_{0}^{l_i}\left(E_i A_i E_{i,0}^2 + E_i I_i K_{i,b}^2 + kG_i A_i \Gamma_i^2\right) dx_i \tag{9}$$

The gravity potential energy of the i[th] link and tip mass is calculated by

$$\begin{aligned} &u_{i,m} = \rho_i A_i g\left(\sum_{j=0}^{i-1} M_j(l_j,t) + \int_0^{l_i} M_i(x_i,t)dx_i\right) \\ &M_i(x_i,t) = x_i \sin(\theta_{i-1}+\theta_i) + \\ &w_i(x_i,t)\cos(\theta_{i-1}+\theta_i) \quad , \; M_0 = 0 \;\; and \;\; \theta_0 = 0 \\ &u_{tip} = m_{tip} g \sum_{j=1}^{N} M_j(l_j,t) \end{aligned} \tag{10}$$

The potential energy due to the gravity is given by

$$U_g = \sum_{i=1}^{N} u_{i,m} + u_{tip} \tag{11}$$

The potential energy stored in the flexible joints can be written as follows

$$U_{flexible\ joints} = \frac{1}{2}\sum_{i=1}^{N} K_i(\theta_i - \theta_{mi})^2 \tag{12}$$

According to presented expressions, the potential energy of the whole system can now be derived as

$$U = SE + U_g + U_{flexible\ joints} \tag{13}$$

3. Derivatives of dynamic model

In this part, the equations of motion of multi-flexible link manipulator with mobile base which incorporate both structural and joint flexibility will be developed. The extended Hamilton method, the Galerkin method, and the mixed finite element formulation are utilized to derive of ordinary differential dynamic equations for system.

3.1 Shear locking and mixed finite element formulation

Shear locking is a numerical problem in structural calculations by finite element methods when the structure looks like a slender beam or shell, the main deformation is bending and there are not enough elements across the thickness. If this occurs then the stiffness of the structure is significantly (orders of magnitude) over predicted (deformation is under predicted) and the shear stresses are predicted much higher than the tensile stress (usually for bending is the other way around). Shear locking occurs than elements are not smart enough to use correct shape for shear stress inside the element (many elements only consider stress to be linear inside the element or even constant) and the difference between the real and approximated by finite element shear stress profile is high. Then the finite element analysis might predict the structure as supported by large shear stresses rather than the tensile stresses (Rakowski 1990). The term mixed method was first used in the 1960's to describe finite element methods in which both bending moment and displacement fields are approximated as primary variables. In this method, shear deformation can be easily included without involving the shear locking in the element and, thus the behavior is independent of the number of integration points along the element. The basic advantages of the mixed method are that the solution of the resulting equations immediately yields moments and displacements and no shear locking is observed in mixed formulation.

Based on the mixed finite element formulation, the finite element approximations for the displacement, rotation, and bending moment field can be introduced as

$$\begin{Bmatrix} \tilde{w}_{i,j} \\ \tilde{\beta}_{i,j} \\ \tilde{M}_{i,j} \end{Bmatrix} = \begin{bmatrix} N_1^d(x) & 0 & 0 & N_2^d(x) & 0 & 0 \\ 0 & N_1^d(x) & 0 & 0 & N_2^d(x) & 0 \\ 0 & 0 & N_1^M(x) & 0 & 0 & N_2^M(x) \end{bmatrix} \{q_{i,j}\} \tag{14}$$

where the shape functions for each field is assumed as

$$\begin{Bmatrix} N_1^d & N_2^d \end{Bmatrix} = \begin{Bmatrix} N_1^M & N_2^M \end{Bmatrix} = \begin{Bmatrix} \left(1-\frac{x}{l}\right) & \frac{x}{l} \end{Bmatrix} \qquad 0 \le x \le l \tag{15}$$

The vector of nodal Dofs of the j[th] beam element from i[th] flexible link is given by

$$\{q_{i,j}\} = \{w_{i,2j-1} \;\; \beta_{i,2j-1} \;\; M_{i,2j-1} \;\; w_{i,2j} \;\; \beta_{i,2j} \;\; M_{i,2j}\}^T \tag{16}$$

where $\tilde{w}_{i,j}, \tilde{\beta}_{i,j}$ and $\tilde{M}_{i,j}$ are the displacement, rotation and bending moment of any arbitrary point of the j[th] element for i[th] flexible link, respectively. Based on the Timoshenko theory of beam, the bending moment for small and large deformation, given by

$$\begin{cases} M = EI\dfrac{\partial\beta(x,t)}{\partial x} \\ \qquad For\ small\ deformation \\ M = EIK^b = EI\dfrac{\partial\beta(x,t)}{\partial x}\left(\cos\beta + \dfrac{\partial w(x,t)}{\partial x}\sin\beta\right) \\ \qquad For\ large\ deformation \end{cases} \tag{17}$$

The stiffness matrix of the base element (e) for large deformation model is presented in Appendix. The set dynamics equation of the N-flexible links and N-flexible joints with mobile base can be obtained in the following form

$$\begin{bmatrix} M_{mb} & 0 \\ 0 & J_{fj} \end{bmatrix}\begin{bmatrix} \ddot{q}_{mb} \\ \ddot{q}_{fj} \end{bmatrix}+\begin{bmatrix} K_{mb} & K_m \\ 0 & -K_{fj} \end{bmatrix}\begin{bmatrix} q_{mb} \\ Q_r - q_{fj} \end{bmatrix}+\begin{bmatrix} h_{mb}(q_{mb},\dot{q}_{mb}) \\ 0 \end{bmatrix}=\begin{bmatrix} \tau_{mb}+A^T\lambda \\ \tau \end{bmatrix} \tag{18}$$

Where

$$\begin{aligned} &for\ i=1:1:3\sum_{r=1}^{N} n_r+4N+5 \\ &for\quad j=1:1:N \\ &if\ q_{mb}(i)=q_j(1) \qquad (K_m)_{ij}=K_j \\ &else \qquad\qquad\quad (K_m)_{ij}=0 \end{aligned} \tag{19}$$

where $K_{fj}=dig[K_1,K_2,\ldots,K_N]$ is a diagonal stiffness matrix modeling the joint elasticity, $J_{fj}=dig[J_1,J_2,\ldots,J_N]$ is the diagonal matrix representing motor inertia, and τ is vector of applied torque to joints. The symbol τ_{mb} is vector of applied torque to driving wheels, A is a matrix derived from the non-holonomic constraints and λ is Lagrange multipliers. $3\sum_{r=1}^{N} n_r+4N+5$ is equal to the total number of degrees of freedom for N-flexible links manipulator. Generalized coordinates based on mixed finite element formulation are chosen as

$$\begin{aligned} &q_{mb}=[x_b \quad y_b \quad \phi \quad \theta_r \quad \theta_l \quad q_1 \quad q_2 \quad \ldots \quad q_i \quad \ldots \quad q_N]^T \\ &q_i=[\theta_i \quad w_{i,1} \quad \ldots \quad w_{i,n_i+1} \quad \beta_{i,1} \quad \ldots \quad \beta_{i,n_i+1} \quad M_{i,1} \quad \ldots \quad M_{i,n_i+1}]^T_{1\times(3n_i+4)} \\ &q_{fj}=[\theta_{m1},\theta_{m2},\ldots,\theta_{mN}]^T \\ &Q_r=[\theta_1,\theta_2,\ldots,\theta_N]^T \end{aligned} \tag{20}$$

where n_i is the number of elements for ith flexible link. In Eq. (18), $[M_{mb}]$ is the nonlinear mass matrix, $[K_{mb}]$ is the stiffness matrix and $h_{mb}(q_{mb},\dot{q}_{mb})$ considering the contribution of other dynamic forces such as centrifugal, Coriolis and gravity forces. The Eq. (19) states that the dimension of the matrix K_m is $\left(3\sum_{r=1}^{N} n_r+4N+5\right)\times N$. Therefore, all elements of the matrix except for the elements related to the link angle is zero and the nonzero elements are equal to $K_i(\theta_i-\theta_{mi})$, $i=1,2,\ldots,N$.

4. Dynamic load carrying capacity of flexible link and flexible joint manipulators

This section presents a general approach to calculate the maximum load based on accuracy, actuator and dynamic stability constraints. For details on the formulation of joint actuator torque and accuracy constraints the reader is referred to Korayem *et al.* (2005).

4.1 Formulation of dynamic stability constraint

To analyze the dynamic stability of a wheeled mobile manipulator on its motion, MHS criterion is used, which has proposed by Moosavian and Alipour (2006). The following steps should be considered to apply MHS measure. First, the mobile manipulator is divided into two subsystems i.e., the mobile base and the manipulator arm(s). Next, all forces and torques exerted to the mobile base are considered. Those forces and torques are coming from the manipulator motion, consisting of gravitational, inertial, and external forces and torques. The support boundary polygon is constituted of the base contact points on the ground. The resultant moment about each edge of support boundary is computed. Then, for each edge of the support polygon, a unit vector, $\hat{a}_i$ is defined such that all the unit vectors make a closed loop direction. Next, the dynamic MHS measure α is calculated as follows

$$\alpha=\min(\alpha_i) \qquad i=1,2,\ldots,n \tag{21}$$

Where α_i denotes the dynamic stability margin about the ith boundary edge and

$$\alpha_i=(I_{vi})^{\sigma_i} M_i.\hat{a}_i \tag{22}$$

where I_{vi} is the base moment of inertia around the ith edge of the support boundary edge, and

$$\sigma_i=\begin{cases} +1 & if\ \ M_i\hat{a}_i \succ 0 \\ -1 & otherwise \end{cases} \tag{23}$$

When the minimum of all α_i is positive, the system is stable, and conversely the negative value of displays the instability is in progress. The zero values of α represents the critical dynamic stability.

For determining the maximum DLCC during a given trajectory, the computational approach summarized as follows:

Step 1: Discretizing the given trajectory into m points and choosing an initial value for $m_{tip}(i)$, i=1.

Step 2: Finding joints variables by solving inverse dynamic for the same rigid links and rigid joints manipulator.

Step 3: Deriving the dynamic equations of motion for manipulator with structural and joint flexibility using extended Hamilton principle.

Step 4: Solving the coupled nonlinear differential Eq. (18) for mobile manipulator.

Step 5: Calculating the no load torque from the joint Eq. (18) and determining the load coefficient c_a based on actuator constraints (Korayem *et al*. 2005).

Step 6: Calculating the no load deflection from the Eq. (18) and determining the load coefficient c_p based on accuracy constraint (Korayem *et al*. 2005).

Step 7: Computing the general load coefficient, c as follows

c=min{c_p, c_a}

Step 8: Putting $m_{tip}(i+1)=cm_{tip}(i)$

Step 9: If $m_{tip}(i+1)$-$m_{tip}(i)\leq$error then DLCC=$m_{tip}(i+1)$, otherwise go to step 4.

Step 10: Considering stability constraint for the computed maximum DLCC from step 9 using MHS criterion.

5. Simulation results

A simulation study has been carried out to show the capability of proposed approach in deriving the equation of motion of flexible link and flexible joint manipulator with mobile base. In addition, the maximum load carrying capacity is investigated for a given trajectory according to the presented strategy.

Case I: In order to check the validity of the model proposed, the mobile two flexible links and rigid joints manipulator problem from Korayem *et al.* (2012) is considered. In this case, the initial coordinates of the end effector are x_1=0.78, y_1=0.35, z_1=1.64 (m) and it must reach the final point with coordinates x_2=3.64, y_2=0.11, z_2=1.9 (m) at t_f=1.8 sec. It is considered that the base moves through clothoid path which its desired trajectory is derived by Fresnel integrals as

$$x_b = \int_0^t \cos\left(\frac{\pi}{2}t^2\right)dt\ , \quad y_b = \int_0^t \sin\left(\frac{\pi}{2}t^2\right)dt$$

The parameters of manipulator and mobile base used in simulation are given in Table 1. The responses of end effector in X, Y and Z directions for both small and large deformation are shown in Figs. 3, 4, and 5, respectively. Also, actual end effector trajectory toward desired trajectory is presented in Fig. 6. In this case, the permissible error bound for the end effector motion around the desired path is

Table 1 Parameters of two link flexible mobile manipulator in clothoid base path (Korayem *et al.* 2012)

Parameter (unit)	Value (manipulator)	Value (base)
Length of links (m)	$l_1 = l_2 = 2.5$	-------
Cross section area (m^2)	$A_1 = A_2 = 9\times10^{-4}$	-------
Mass (kg)	$m_1 = m_2 = 5$	$m_{base} = 55$
Moment of inertia (m^4)	$I_1 = I_2 = 15\times10^{-8}$	$I_{base} = 0.2$
Young's modulus of material (N/m^2)	$E_1 = 70\times10^9$, $E_2 = 45\times10^9$	-------

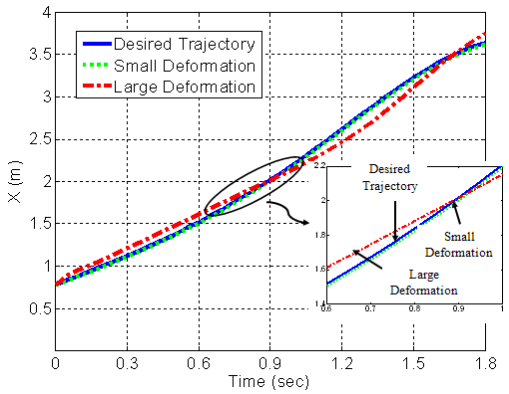

Fig. 3 Trajectory of end effector in X direction

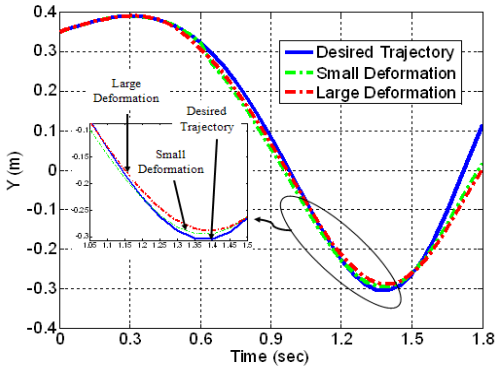

Fig. 4 Trajectory of end effector in Y direction

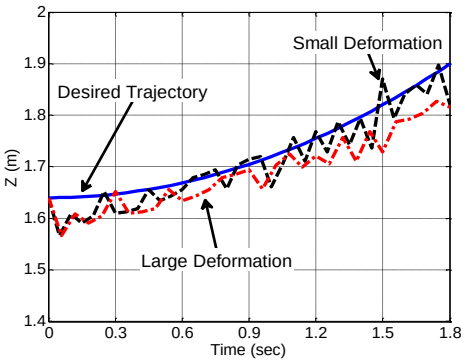

Fig. 5 Trajectory of end effector in Z direction

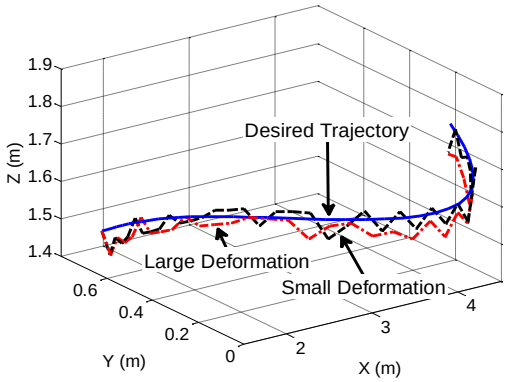

Fig. 6 The desired and actual trajectory

R_p=12 cm and actuators of the robot are considered with τ_s=385 N.m and ω_n=10 rad/s. The maximum DLCC, by imposing both accuracy and joints torque constraints, is 1.82 kg. The results obtained are in good agreement with presented results by (Korayem *et al.* 2012).

Case II: According to second study, a circular trajectory is selected for tracking problem of two flexible link and flexible joint manipulator with wheeled mobile base. Equations of desired circular trajectory that must be happened in 6 seconds are presented in Table 3. The base is forced to move on a predefined trajectory. It is considered that the base moves from the origin to point (0.45, 0.195) and then returns to the origin. All necessary parameters for computational simulation can be found in Table 2.

Table 2 Parameters of two flexible link and flexible joint manipulator

Parameter	Value (unit)
Length of links	$l_1 = 0.4$ m , $l_2 = 1.6$ m
Density of links	$\rho_1 = \rho_2 = 3000\ kg/m^3$
Young's modulus of material	$E_1 = E_2 = 0.3\times10^{11}\ N/m^2$
Spring constant	$K_1 = K_2 = 600\ N/m$
Cross section area	$A_1 = A_2 = 2.5\times10^{-3}\ m^2$
Moment of inertia	$I_1 = I_2 = 5.2\times10^{-7}\ m^4$
Shear modulus of material	$G_1 = G_2 = 16\times10^{6}\ N/m^2$
Motor's moment of inertia	$J_1 = J_2 = 0.5\ kgm^2$
Mass of base	$m_{base} = 65$ kg
Base's moment of inertia	$I_{base} = 0.297\ m^4$

Table 3 Reference input for mobile manipulator

$t \le 3$	$3 < t \le 6$
$xe = (2.2 - 0.2\cos(\frac{\pi}{9}t^2))\cos(\frac{\pi}{8})$	$xe = (2.2 - 0.2\cos(\frac{\pi}{9}(-t+6)^2))\cos(\frac{\pi}{8})$
$ye = (2.2 - 0.2\cos(\frac{\pi}{9}t^2))\sin(\frac{\pi}{8})$	$ye = (2.2 - 0.2\cos(\frac{\pi}{9}(-t+6)^2))\sin(\frac{\pi}{8})$
$ze = 0.2\sin(\frac{\pi}{9}t^2)$	$ze = -0.2\sin(\frac{\pi}{9}(-t+6)^2)$

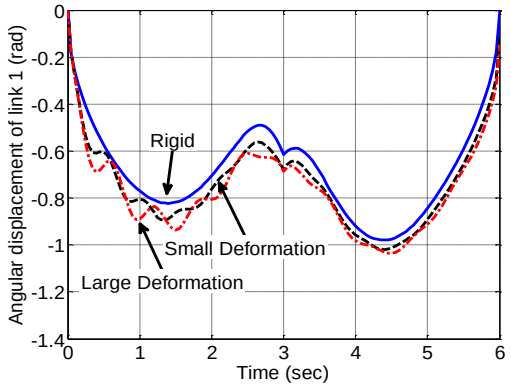

(a) First link

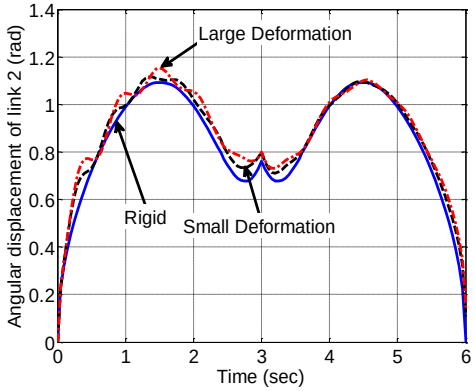

(b) Second link

Fig. 7 Angular positions of links under rigid, small and large deformation models

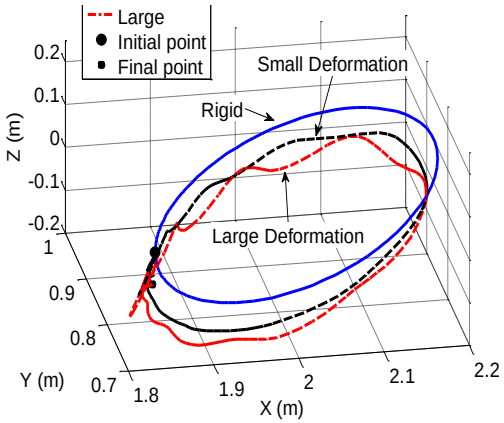

Fig. 8 End effector trajectory in XYZ plane

For an allowable tracking error equal to 10 cm, DLCC of robot is 1.85 kg. Maximum DLCC of the mobile manipulator considering joints torque constraint is found to be 2.7 kg. By considering stability constraint based on MHS criterion and tip mass equals to 1.85 kg, dynamic MHS measure is negative and this means that mobile manipulator under this tip mass is capsized. Therefore, maximum DLCC of the mobile manipulator considering stability constraint is 1.5 kg. The angular displacement of two links is shown in Fig. 7. The end effector trajectories obtained for full load conditions are shown in Fig. 8. The configuration of the mobile manipulator with full load is demonstrated in Fig. 9. For the triangular support boundary polygon, Moment-Height criteria related to the different edges of support polygon is shown in Fig. 10. According to the descriptions given in subsection 4-1 about stability constraint, when the minimum of all dynamic stability margins is positive, the system is stable. Fig. 10 shows that all dynamic stability margins are positive and therefor this plot represents that stability is guaranteed. Fig. 11 shows the angular positions of system with different values of torsional spring constant. This figure indicates joints elastic deformation with large spring constant vanishes. Fig. 12 represents the angular response of links and motors based on large deformation model.

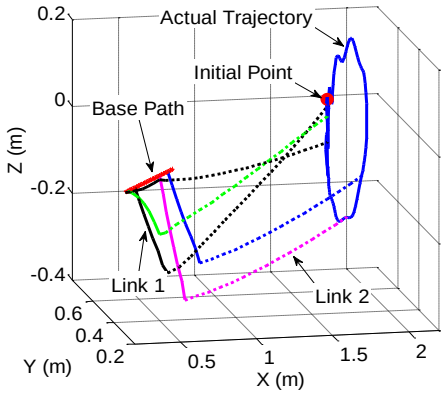

Fig. 9 The configuration of the mobile manipulator with full load

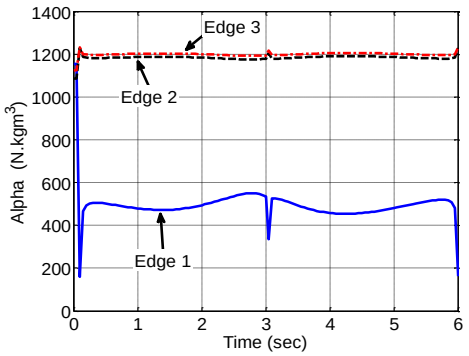

Fig. 10 The MHS measure related to the different edges of the support polygon

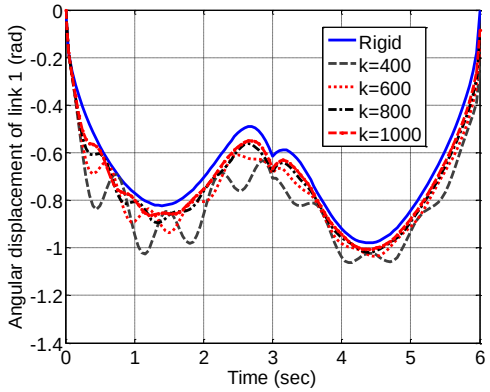

(a) First link

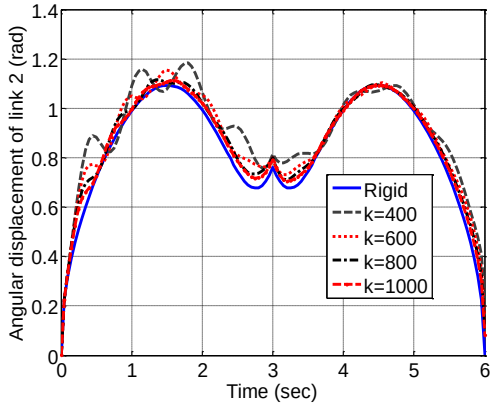

(b) Second link

Fig. 11 Angular positions of links with different values of torsional spring constant

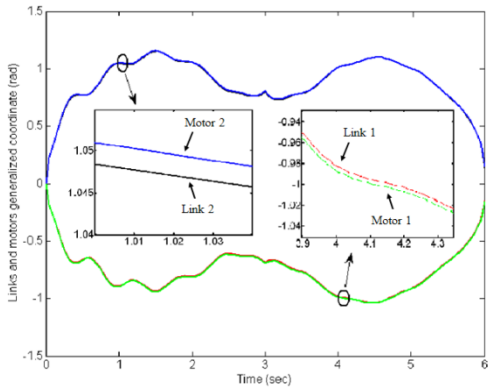

Fig. 12 Angular positions of the joints and motors

6. Experimental results

The experimental setup presented in Fig. 13 is consisted of a two flexible link manipulator. The first joint is driven by a servo-tech AC servo motor and the second joint driven by a DC motor. An incremental encoder with the resolution of 2500 pulse per revolution is used to measure the rotational position of the first motor. The rotational position of the second motor is measured by a small absolute magnetic encoder. The deflection of each point of both links is estimated by the data obtained from three strain gauge bridges mounted on the both sides of the links. The flexible manipulator has a planar motion, thus the effect of gravity can be ignored. The physical parameters of the flexible links are shown in Table 4. In order to obtain maximum dynamic load of the planar flexible robot manipulator, angular positions of links are considered similar to Fig. 14. Actuators of the robot are considered by τ_s=0.1 N.m and maximum allowable dynamic load of the manipulator considering torque constraint is 0.62 kg for the given path. The actual path tracked by the planar manipulator is compared with the desired path in Fig. 15. In Fig. 16, the torques applied to the links corresponding to the experimental setup and numerical simulation is presented. This figure represents that the first arm torque will reach to the saturation sooner than the torque obtained by second arm. By studying the figures related to angular displacement and arms torque, it is clear that, change in angular displacement of the arms at t=2.5 sec will cause to alter the applied torques.

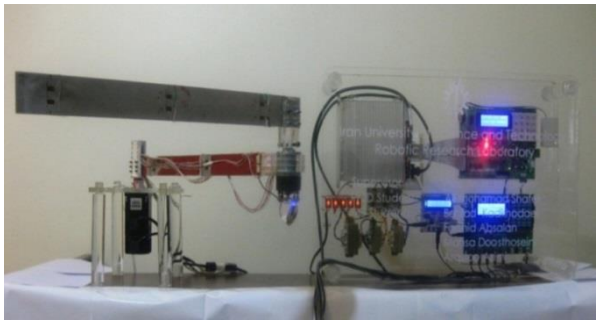

Fig. 13 Two link flexible robotic manipulator (experimental setup)

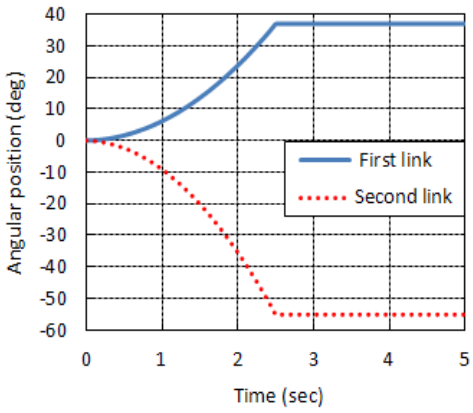

Fig. 14 Angular position for both the first and second links

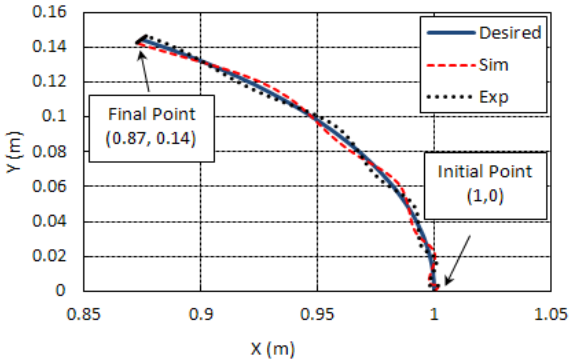

Fig. 15 End effector trajectory in XY plane

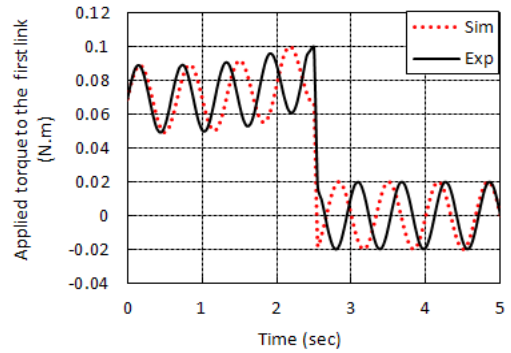

(a) First link

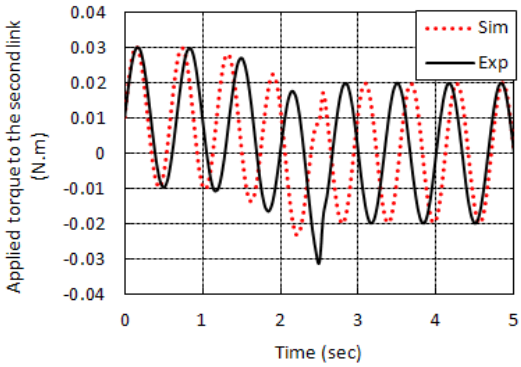

(b) Second link

Fig. 16 Applied torques to the first and second links

Table 4 Physical parameters of the experimental setup

Parameters	Value (unit)
Length of the links	$l_1 = l_2 = 0.5\ m$
Height of the links	$h_1 = 4;\ h_2 = 5.17\ cm$
Thickness of the links	$t_1 = 4;\ t_2 = 1.5\ mm$
Bending stiffness	$EI_{z1} = 14.93;\ EI_{z2} = 1.017\ \ \mathrm{N.m^2}$
Mass per unit length	$\mu_1 = 0.504;\ \mu_2 = 0.2442\ \ Kg/m$
Mass moment of inertia per unit length	$J_1 = \begin{bmatrix} 0.584 & 0 & 0 \\ 0 & 0.578 & 0 \\ 0 & 0 & 0.00578 \end{bmatrix} \times 10^{-4}\ \ Kg/m$ $J_2 = \begin{bmatrix} 0.4685 & 0 & 0 \\ 0 & 0.4681 & 0 \\ 0 & 0 & 0.0004 \end{bmatrix} \times 10^{-4}\ \ Kg/m$
Mass of the DC motor	$M_{m_1} = 0.495\ \ \mathrm{Kg}$

7. Conclusions

A generalized modeling framework has been described to obtain the closed form of nonlinear dynamic equations of motion for mobile base multi-link manipulator with a tip mass considering the flexibility in the links and joints by using extended Hamilton principle and Galerkin discretization technique. To include the effects of shear and rotational inertia, TBT has been applied. In order to overcome shear locking phenomena in elements, a new procedure has been employed based on mixed finite element formulation. The emphasis of this paper has been set on precise and complete dynamic analysis of flexible links and flexible joints manipulator with mobile base including large deformation conditions. The dynamic model of the manipulator in this paper has considered large deformation of the links due to geometrically nonlinear behavior, dynamics of load and manipulator, joints flexibility, gravity, and mobile base subject to non-holonomic constraints. Another purpose of this work was to determine dynamic load carrying capacity of the mentioned flexible manipulator as an important characteristic of a manipulator. In addition, for a wheeled mobile robot, dynamic stability constraint was discussed by applying MHS approach. Numerical simulations were carried out for various end effector trajectories observing the flexible deformations produced by the joints and the links make it difficult for the end effector to track a prescribed trajectory accurately. The results represent that dynamic stability constraint is dominant constraint for the given circular path and the maximum allowable dynamic load of the manipulator considering all constraints is 1.5 kg. In addition, by changing the trajectory of end effector, maximum load also changes. As for clothoid path, maximum load of the manipulator is equal to 1.82 kg and DLCC is 1.5 kg considering circular trajectory. It has been found that dynamic behavior of manipulators with structural and joint flexibility considering larger values of the torsional spring constant are correlated with response of flexible link and rigid joint manipulators. Fluctuation range in obtained figures for angular displacement of links and end effector path is bigger for large deformation model (See Figs. 7-8). Theoretically dynamic model is validated by an experiment on a two flexible link and rigid joint manipulator. The comparisons demonstrate that the mixed formulation is reliable and so it can be trusted in multi-flexible link manipulators. For future study, the achieved results from the proposed method can be compared with industrial robot experimental results (e.g., Scout mobile robot). Also, for improving joint modeling, besides flexibility, the effects of damping and friction can also be included.

References

Aarts, R.G.K.M. and Jonker, J.B. (2002), "Dynamic simulation of planar flexible link manipulators using adaptive modal integration", *Multi-body Syst. Dyn.*, **7**(1), 31-50.

Ailon, A. (1998), "An approach for set-point regulation of electrically driven flexible-joint robots with uncertain

parameters", *The IEEE International Conference on Control Applications*, 882-886.
Bayo, E. (1989), "Timoshenko versus Bernoulli-Euler beam theories for inverse dynamics of flexible robots", *Int. J. Robotics Automat.*, **4**(1), 53-56.
Beirao da Veiga, L., Lovadina, C. and Reali, A. (2012), "Avoiding shear locking for the Timoshenko beam problem via isogeometric collocation methods", *Comput. Method. Appl. Mech. Eng.*, **241**, 38-51.
Desai, J.P. and Kumar, V. (1999), "Motion planning of non-holonomic cooperating mobile manipulators", *J. Robotic Syst.*, **16**(10), 557-579.
Dmitrochenko, O. (2008), "Finite elements using absolute nodal coordinates for large deformation flexible multi-body dynamics", *J. Comput. Appl. Math.*, **215**(2), 368-377.
Dombrowski, S.V. (2002), "Analysis of large flexible body deformation in multi-body systems using absolute coordinates", *Multi-body Syst. Dyn.*, **8**(4), 409-432.
Dwivedy, S.K. and Eberhard, P. (2006), "Dynamic analysis of flexible manipulators, a literature review", *Mechanism and Machine Theory*, **41**(7), 749-777.
Fukuda, T., Fujisawa, Y., Muro, E., Hoshino, H., Otubo, K., Uehara, K., Kosuge, K., Arai, F. and Miyazaki, T. (1992), "Manipulator/vehicle system for man-robot cooperation", *The IEEE international conference on robotics and automation*, 74-79.
Ghasempoor, A. and Sepehri, N. (1995), "A measure of stability for mobile based manipulators", *The IEEE international conference on robotics and automation*, 2249-2254.
Huang, Q., Tanie, K. and Sugano, S. (2000), "Coordinated motion planning for a mobile manipulator considering stability and manipulation", *Int. J. Robotic. Res.*, **19**(8), 732-742.
Iwai, R. and Kobayashi, N. (2003), "A new flexible multi-body beam element based on the absolute nodal coordinate formulation using the global shape function and the analytical mode shape function", *Nonlinear Dyn.*, **34**, 207-232.
Kim, J., Chung, W.K., Youm. Y. and Lee, B.H. (2002), "Real time ZMP compensation method using null motion for mobile manipulator", *The IEEE international conference on robotics and automation*, 1967-1972.
Korayem, M.H. and Ghariblu, H. (2004), "The effect of base replacement on the dynamic load carrying capacity of robotic manipulators", *Int. J. Adv. Manufact. Technol*., **23**(1-2), 28-38.
Korayem, M.H., Haghpanahi, M. and Heidari, H.R. (2012), "Analysis of flexible mobile manipulators undergoing large deformation with stability consideration", *Latin Am. Appl. Res.*, **42**(2), 111-119.
Korayem, M.H. and Basu, A. (1994), "Dynamic load carrying capacity of robotic manipulators with joint elasticity imposing accuracy constraints", *Robot. Autonomous Syst.*, **13**(3), 219-229.
Korayem, M.H. and Heidari, A. (2007), "Maximum allowable dynamic load of flexible mobile manipulators using finite element approach", *Int. J. Adv. Manufact. Technol*., **36**(9), 606-617.
Korayem, M.H. and Shokri, M. (2008), "Maximum dynamic load carrying capacity of a 6 ups-Stewart platform manipulator", *Scientia Iranica*, **15**(1), 131-143.
Korayem, M.H., Ghariblu, H. and Basu, A. (2005), "Dynamic load-carrying capacity of mobile base flexible joint manipulators", *Int. J. Adv. Manufact. Technol*., **25**(1), 62-70.
Korayem, M.H., Haghpanahi, M. and Heidari, H.R. (2010), "Maximum allowable dynamic load of flexible manipulators undergoing large deformation", *Scientia Iranica*, **17**(1), 61- 74.
Kubler, L., Eberthard, P. and Geisler, J. (2003), "Flexible multi-body systems with large deformations and nonlinear structural damping using absolute nodal coordinates", *Nonlinear Dyn.*, **34**(1-2), 31-52.
Lin, Y.J. and Gogate, S.D. (1989), "Modeling and motion simulation of an n-link flexible robot with elastic joints", *The International Symposium on Robotics and Manufacturing*, Santa Barbara, CA, 39-43.
Liu, J., Hong, J. and Cui, L. (2007), "An exact nonlinear hybrid-coordinate formulation for flexible multi-body systems", *Acta Mechanica Sinica*, **23**(6), 699-706.
Moosavian, S.A.A. and Alipour, K. (2006), "Stability evaluation of mobile robotic systems using moment- height measure", *The IEEE International Conference on Robotics, Automation and Mechatronics*, Bangkok, 1-6.
Papadopoulos, E. and Ray, D. (1996), "A new measure of tip over stability margin for mobile manipulators", *The IEEE international conference on robotics and automation*, 3111-3116.
Rakowski, J. (1990), "The interpretation the shear locking in beam elements", *Comput. Struct.*, **37**(5), 769-776.
Shabana, A.A. (1998), "Computer Implementation of the absolute nodal coordinate formulation for flexible multi-body dynamics", *Nonlinear Dyn.*, **16**(3), 293-306.
Subudhi, B. and Morris, A.S. (2002), "Dynamic modeling, simulation and control of a manipulator with flexible links and joints", *Robot. Autonomous Syst.*, **41**(4), 257-270.
Sweet, L.M. and Good, M.C. (1984), "Re-definition of the robot motion control problem: effects of plant dynamics, drive systems, constraints and user requirement", *The 23rd IEEE Conference on Decision and Control*, Las Vegas, NV, 724-731.
Thomas, M., Yuan-Chou, H.C. and Tesar, D. (1985), "Optimal actuator sizing for robotic manipulators based on local dynamic criteria", *J Mech. Trans. Auto. Des.*, ASME, **107**, 163-169.
Vallejo, D.G., Escalona, J.L., Mayo, J. and Dominguez, J. (2003), "Describing rigid-flexible multi-body systems using absolute coordinates", *Nonlinear Dyn.*, **34**(1), 75-94.
Wang, L.T. and Ravani, B. (1988), "Dynamic load carrying capacity of mechanical manipulators - part I: Problem formulation", *Trans. J. Dyn. Syst., Measure. Control*, ASME, **110**, 46-52.
Yang, G.B. and Donath, M. (1988), "Dynamic model of a two link robot manipulator with both structural and joint flexibility", *The ASME 1 Winter Annual Meeting*, Chicago, IL, 37-44.
Yuan, K. and Lin, L. (1990), "Motor-based control of manipulators with flexible joints and links", *Proceedings of the IEEE International Conference on Robotics and Automation*, 1809-1814.
Yue, S. and Tso, S.K. (2001), "Maximum dynamic payload trajectory for flexible robot manipulators with kinematic redundancy", *Mech. Machine Theory*, **36**(6), 785-800.
Yue, S.G., Yu, Y.Q. and Bai, S.X. (1997), "Flexible rotor beam element for robot manipulators with link and joint flexibility", *Mech. Machine Theory*, **32**(2), 209-219.

CC

Nomenclature

(θ_r, θ_l)	Coordinates of the driving wheels
r	Radius of the driving wheels
m_{base}	Mass of the mobile base
I_{base}	Moment of inertia for the mobile base
(x_b, y_b)	Translation coordinates of the moving platform
ϕ	Rotation coordinate of the moving platform
J_r, J_l	Driving wheels moment of inertia
$\lfloor E_{ij} \rfloor$	Green-Lagrange strain tensor
$\lfloor S_{ij} \rfloor$	Second Piola-Kirchoff stress tensor
E_i	Young's modulus of ith link
G_i	Shear modulus of ith link
A_i	Cross sectional area of ith link
I_i	Moment of inertia of the cross section for ith link
l_i	Length of ith link
ρ_i	Density of ith link
K_i	Spring constant of ith elastic joint
J_i	Moment of inertia for ith motor
k	Shear correction factor
g	Gravity acceleration
L	The distance between driving wheels
d	The distance between driving wheels and center of mobile platform
m_{tip}	Tip mass
θ_f	Coordinate of the driver wheel
q_{mb}	Generalized coordinate of N-flexible links and N-rigid joints mobile manipulator
q_i	Degrees of freedom for ith flexible link
q_{fj}	Generalized coordinate of the flexible joints
Q_r	Generalized coordinate of the flexible links

Appendix

The stiffness matrix of the base element (e) for large deformation model is by

$$[K]^{(e)} = \begin{bmatrix} k_{11} & k_{12} & k_{13} \\ k_{21} & k_{22} & k_{23} \\ k_{31} & k_{32} & k_{33} \end{bmatrix} \tag{A-1}$$

when the mechanical and geometrical properties are constant along the beam, the sub matrices for the base element (e) are

$$\begin{aligned}
[k_{11}]_{ij} &= -3EA\int_0^l \left\{ \frac{d\left(N_i^d \left(\frac{\partial w}{\partial x} \right)^2 \right)}{dx} \frac{dN_j^d}{dx} \right\} dx - \\
& kGA\int_0^l \left\{ \frac{d\left(N_i^d \cos^2\beta \right)}{dx} \frac{dN_j^d}{dx} \right\} dx \\
[k_{12}]_{ij} &= kGA\int_0^l \left\{ N_i^d \frac{dN_j^d}{dx} \cos 2\beta \right\} dx + \\
& kGA\int_0^l \left\{ N_i^d \frac{dN_j^d}{dx} \frac{\partial w}{\partial x} \sin 2\beta \right\} dx \\
[k_{13}]_{ij} &= 2\int_0^l \left\{ N_i^d \frac{dN_j^M}{dx} \frac{\partial \beta}{\partial x} \sin\beta \right\} dx - \\
& 2\int_0^l \left\{ \frac{d\left(N_i^d N_j^M \sin\beta \right)}{dx} \frac{\partial \beta}{\partial x} \right\} dx + 2\int_0^l \left\{ N_i^d N_j^M \left(\frac{\partial \beta}{\partial x} \right)^2 \cos\beta \right\} dx \\
[k_{21}]_{ij} &= kGA\int_0^l \left\{ N_i^d \frac{dN_j^d}{dx} \cos 2\beta \right\} dx \quad , \\
[k_{22}]_{ij} &= 2EI\int_0^l \left\{ N_i^d \frac{dN_j^d}{dx} \cos\beta K_b \frac{\partial w}{\partial x} \right\} dx \\
[k_{23}]_{ij} &= 2\int_0^l \left\{ N_i^d \frac{dN_j^M}{dx} \left(\cos\beta + \frac{\partial w}{\partial x} \sin\beta \right) \right\} dx - \\
& 2\int_0^l \left\{ \frac{d\left(N_i^d N_j^M \right)}{dx} \frac{\partial w}{\partial x} \sin\beta \right\} dx \quad , \quad [k_{31}]_{ij} = 0 \\
[k_{32}]_{ij} &= -EI\int_0^l \left\{ N_i^M \frac{dN_j^d}{dx} \left(\cos\beta + \frac{\partial w}{\partial x} \sin\beta \right) \right\} dx \quad , \\
[k_{33}]_{ij} &= \int_0^l \left\{ N_i^M N_j^M \right\} dx \qquad i, j = 1,2
\end{aligned} \tag{A-2}$$